Galvanomagnetic Tensor of Bismuth at 20.4°K*

SHOICHI MASE
Kyushu University, Fukuoka, Japan

AND

S. VON MOLNAR AND A. W. LAWSON
University of California, Riverside, California

(Received March 8, 1962)

Theoretical expressions for the conductivity tensors of semimetals are derived using the deformation potential approach and are compared with experimental values for zone-refined bismuth at 20.4°K in fields up to 7000 Oe. The agreement is reasonably satisfactory if one assumes only one light-hole band. The data appear to be quite inconsistent with the existence of an additional heavy-hole band, unless we assume an extremely small deformation potential for the heavy hole. Numerical values for the relaxation times and the deformation potential are derived from the experimental results.

I. INTRODUCTION

BOTH experimental[1] and theoretical studies[2] have been carried out on the galvanomagnetic effects in bismuth. However, adequate experiments on the anisotropy of these phenomena have been primarily confined to the case of weak magnetic fields for which $\omega_c\tau \ll 1$, where ω_c is the cyclotron frequency and τ is the relaxation time. These results have been explained reasonably well in terms of the many-valley model.[3]

The previous determinations of the tensor components in weak fields have been made mostly in the range from liquid nitrogen to room temperature, where the condition $\omega_c\tau \ll 1$ is easy to satisfy for reasonable magnetic field strengths. This temperature range, however, is not necessarily favorable from a theoretical point of view for the following two reasons. Firstly, this temperature range brackets the Debye characteristic temperature Θ_D which is 119°K in bismuth.[4] It is, therefore, questionable to treat the electron-phonon interaction in the usual simple approximation because the frequency spectrum of the lattice may be complicated for large wave numbers and because both acoustical and optical phonons may be excited. To take full account of the exact spectrum and all types of scattering mechanisms is, however, difficult. Secondly, the occupation of the energy band in this temperature region may be quite different from that at very low temperatures, because a considerable number of electrons in the valence band are thermally excited to the conduction band. At the present time, most of our detailed knowledge of the band structure in Bi is based on low-temperature experiments such as the cyclotron absorption and the de Haas-van Alphen type oscillations. It is hardly possible to calculate every physical quantity from first principles only, and we must use available experimental data for parameters in the calculation of the galvanomagnetic tensors. Thus, it is clear that focusing our attention on low temperatures is more useful.

We should point out, however, that in the liquid helium temperature range there is another difficulty in interpreting experimental results, because several kinds of scattering mechanisms become equally important. Although it might be possible to make scattering by impurities predominant by doping, a much simpler way of achieving our objective is to work in an intermediate temperature range near 20°K. This temperature may be high enough to permit the neglect of scattering by static imperfections in good single crystals but low enough to permit the neglect of thermal excitation of the electrons, the high-frequency acoustical phonons, and optical phonons. The most important experimental advantage is that the data in this case should reveal the intrinsic properties of bismuth except for the antisymmetric part of the tensor which is impurity dependent.

Here we present an experimental and theoretical study on the anisotropy of the galvanomagnetic tensor at liquid hydrogen temperature and in strong magnetic fields ranging from 1.5 kOe to 7.3 kOe. In Secs. II and III, a theoretical formulation of the galvanomagnetic effects in semimetals in strong magnetic fields is presented. In Sec. IV, we write down an interpolation formula for the conductivity tensor for intermediate fields, which is needed for the interpretation of the antisymmetric part. In Sec. V, we present the experimental results for all typical tensor components and the angular dependence of the tensor at fixed magnetic field. In Sec. VI, we analyze our data using the theoretical formulation given in Secs. III and IV.

* The experimental work reported here was carried out at the University of Chicago during the spring of 1961. The authors gratefully acknowledge the support of the National Science Foundation at that institution and its continued support at University of California, Riverside, which enabled this work to be completed.

[1] P. B. Alers and R. T. Webber, Phys. Rev. **91**, 1060 (1953); J. M. Reynolds, H. W. Hemstreet, T. E. Leinhart, and D. D. Triantos, *ibid.* **96**, 1203 (1954); R. A. Connell and J. A. Marcus, *ibid.* **107**, 940 (1957); J. Babiskin, *ibid.* **107**, 981 (1957); T. Okada, J. Phys. Soc. Japan **12**, 1327 (1957).

[2] B. Davydov and I. Pomeranchuk, J. Phys. (U.S.S.R.) **2**, 147 (1940).

[3] B. Abeles and S. Meiboom, Phys. Rev. **101**, 544 (1956).

[4] I. N. Kalinkina and P. G. Strekov, Soviet Phys.—JETP **7**, 426 (1958); N. E. Phillips, Phys. Rev. **118**, 644 (1960).

II. THE HAMILTONIAN

A. Energy Eigenvalues and Eigenfunctions

We assume ellipsoidal energy surfaces and the effective mass approximation, although some recent studies show the need of a generalization to more complicated energy surfaces.[5] The energy band is written as

$$\begin{aligned} &E_l=\Delta_l+(g_l/2m)\mathbf{P}\cdot\boldsymbol{\alpha}\cdot\mathbf{P},\\ &\Delta_l=0,\quad g_l=1 \text{ for electrons},\\ &\Delta_l=\Delta,\quad g_l=-1 \text{ for holes}. \end{aligned} \tag{2.1}$$

Δ is the overlapping energy of the conduction and valence bands. As usual we take one of binary axes and the trigonal axis to be the x and the z axis, respectively. One of the bisectrices is then the y axis. The theory, however, does not require any special assumption, except ellipticity, until the final stage.

We assume the magnetic field $\mathbf{H}$ to be parallel to the z axis. The results in other cases are obtained by cyclic permutation of the coordinates x, y, and z. The vector potential $\mathbf{A}$ is taken to be

$$\mathbf{A}=H(0,y,0).$$

The effective mass equation

$$\mathcal{H}_l\psi_l=\mathcal{E}_l\psi_l, \tag{2.2}$$

where

$$\mathcal{H}_l=\Delta_l+(g_l/2m)(\mathbf{P}+g_l|e|\mathbf{A}/c)\cdot\boldsymbol{\alpha}\cdot(P+g_l|e|\mathbf{A}/c),$$

is solvable by putting

$$\psi(\mathbf{r})=\exp[i(k_y y+k_z z)]\exp[iQ_l(x)]\phi_l(x). \tag{2.3}$$

The phase factor $Q_l(x)$ is taken as

$$Q_l(x)=-g_l\frac{1}{2}\frac{m\omega_0}{\hbar}\frac{\alpha_{xy}{}^l}{\alpha_{xx}{}^l}\left(x+g_l\frac{\hbar k_y}{m\omega_0}+g_l\frac{\alpha_{zx}{}^l}{\alpha_{xy}{}^l}\frac{\hbar k_z}{m\omega_0}\right)^2, \tag{2.4}$$

where $\omega_0=|e|H/mc$, the cyclotron frequency of a free electron. By using the above expression for $Q_l(x)$ and the following substitutions:

$$\begin{aligned} &x_0{}^l=-g_l\frac{\hbar}{m\omega_0}\left[k_y+\frac{\alpha_{xx}{}^l\alpha_{yz}{}^l-\alpha_{xy}{}^l\alpha_{zx}{}^l}{[\omega_l(z)/\omega_0]^2}k_z\right],\\ &s_l=\alpha_{xx}{}^{l-\frac{1}{2}}(\omega_l(z)/\omega_0)^{\frac{1}{2}}(m\omega_0/\hbar)^{\frac{1}{2}}x,\\ &\epsilon_l=\Delta_l+g_l(\epsilon_\perp{}^l+\epsilon_{11}{}^l),\\ &\epsilon_\perp{}^l=(n+\tfrac{1}{2})\hbar\omega_l(z),\\ &\epsilon_{11}{}^l=\det\boldsymbol{\alpha}^l(\omega_l(z)/\omega_0)^{-2}(\hbar k_z{}^2/2m)\equiv\lambda_z\hbar k_z{}^2/2m,\\ &\omega_l(z)/\omega_0=(\alpha_{xx}{}^l\alpha_{yy}{}^l-\alpha_{xy}{}^{l2})^{\frac{1}{2}}, \end{aligned} \tag{2.5}$$

we obtain the wave equation for a one-dimensional harmonic oscillator centered at the point $x_0{}^l$,

$$-\frac{d^2\phi^l}{ds_l{}^2}+(s_l-s_0{}^l)^2\phi^l=\frac{2\epsilon_\perp{}^l}{\hbar\omega_l(z)}\phi^l. \tag{2.6}$$

ϕ^l normalized in unit length (approximately equal to the normalization in infinite length) is given by

$$\begin{aligned} \phi_n{}^l(x-x_0{}^l)&=(s_l/x)^{\frac{1}{2}}\pi^{-\frac{1}{4}}(2^n n!)^{-\frac{1}{2}}\exp[-(s_l-s_0{}^l)^2/2]\\ &\quad\times H_n(s_l-s_0{}^l)\\ &\equiv(s_l/x)^{\frac{1}{2}}\Phi_n(s_l-s_0{}^l). \end{aligned} \tag{2.7}$$

$Q_l(x)$ is rewritten in term of a center $x_0{}^l$ as

$$\begin{aligned} Q_l(x-x_0{}^l)=&-g_l\frac{1}{2}\frac{\alpha_{xy}{}^l}{\alpha_{xx}{}^l}\frac{m\omega_0}{\hbar}\\ &\times\left(x-x_0{}^l-g_l\frac{\alpha_{xx}{}^l(\alpha_{xy}{}^l\alpha_{yz}{}^l-\alpha_{yy}{}^l\alpha_{zx}{}^l)}{\alpha_{xy}{}^l[\omega_l(z)/\omega_0]^2}\frac{\hbar k_z}{m\omega_0}\right)^2. \end{aligned} \tag{2.4}'$$

The electronic state is specified by the band index l and the quantum number $q(n,x_0{}^l,k_z)$. Here we consider only intraband transitions and drop the band index l until necessary; we also measure the energy ϵ_l from the bottom or the top of the energy bands.

B. Perturbation Potential

We limit our interest to relatively low temperatures and then take into account only scattering by long-wavelength acoustical phonons and neglect the interband and intervalley transitions. Above liquid-air temperature, however, these interband transitions may play a very important role in scattering mechanisms in view of the low Debye temperature in Bi.

The deformation potential due to the lattice vibrations[6] is given by

$$\delta V=D\sum_{i,j}c_{ij}\epsilon_{ji}, \tag{2.8}$$

where D is the isotropic deformation potential constant which is common to all bands, $\epsilon_{ij}=1/2(\partial u_i/\partial x_j+\partial u_j/\partial x_i)$ the strain tensor component, and c_{ij} a dimensionless factor giving the anisotropy of the deformation potential. c_{ij} has the same symmetry as α_{ij}.

The displacement vector $\mathbf{u}(\mathbf{r})$ is given by

$$\begin{aligned} \mathbf{u}(\mathbf{r})=&(\hbar/2MN)^{\frac{1}{2}}\sum_s\sum_{\mathbf{f}}(\mathbf{e}^{(s)}/\Omega_s)^{\frac{1}{2}}\\ &\times(b_{\mathbf{f}}{}^{(s)}e^{i\mathbf{f}\cdot\mathbf{r}}+b_{\mathbf{f}}{}^{(s)*}e^{-i\mathbf{f}\cdot\mathbf{r}}), \end{aligned} \tag{2.9}$$

where $\mathbf{e}^{(s)}$ is the unit polarization vector and $s=1, 2, 3$, the three directions of the polarization of acoustical phonons. By using the polar angles θ, φ as in Fig. 1, the components of $\mathbf{e}^{(s)}$ can be written as

$$\begin{aligned} &e_x{}^{(1)}=\sin\theta\cos\varphi, \quad e_x{}^{(2)}=-\cos\chi\cos\theta\cos\varphi+\sin\chi\sin\varphi,\\ &e_y{}^{(1)}=\sin\theta\sin\varphi, \quad e_y{}^{(2)}=-\cos\chi\cos\theta\sin\varphi-\sin\chi\cos\varphi,\\ &e_z{}^{(1)}=\cos\theta, \quad e_z{}^{(2)}=\cos\chi\sin\theta. \end{aligned} \tag{2.10}$$

[5] M. H. Cohen, Phys. Rev. **121**, 387 (1961).

[6] J. Bardeen and W. Shockley, Phys. Rev. **80**, 72 (1950).

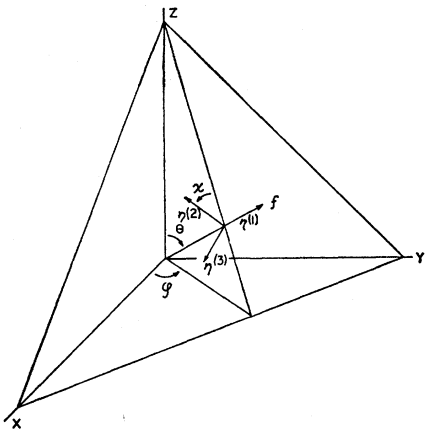

FIG. 1. Polarization vectors.

$\mathbf{e}^{(3)}$ is obtained by replacing χ in $\mathbf{e}^{(2)}$ by $\chi+\pi/2$. $b_{\mathbf{f}}{}^{(s)}$ and $b_{\mathbf{f}}{}^{(s)*}$ are the annihilation and creation operators of the phonon state $\mathbf{f}$ in the branch s. MN is the mass density of the lattice. Then, δV consists of three parts (one longitudinal and two transverse), i.e.,

$$\delta V=\sum_s \delta V_s =i(\hbar D^2/2MN)^{\frac{1}{2}}\sum_s\sum_{\mathbf{f}}(fF_s/\Omega_s{}^{\frac{1}{2}}) \times(b_{\mathbf{f}}{}^{(s)}e^{i\mathbf{f}\cdot\mathbf{r}}-b_{\mathbf{f}}{}^{(s)*}e^{-i\mathbf{f}\cdot\mathbf{r}}), \quad (2.11)$$

where F_s is a dimensionless factor defined as

$$F_s=\sum_{i,j} c_{ij}(e_i{}^{(s)}f_j+e_j{}^{(s)}f_i)/2f. \quad (2.12)$$

In the following we assume the simplest dispersion formula

$$\Omega_s=v_s f, \quad (2.13)$$

where v_s is an f-independent sound velocity and $v_1\neq v_2=v_3$.

C. Hamiltonian and Scattering Probability

The Hamiltonian for the lth band in the absence of an electric field is

$$\mathcal{H}=\mathcal{H}_0+\mathcal{H}', \quad (2.14)$$

where

$$\mathcal{H}_0=\sum_q \epsilon_q a_q{}^* a_q+\sum_s\sum_{\mathbf{f}}(b_{\mathbf{f}}{}^{(s)*}b_{\mathbf{f}}{}^{(s)}+\tfrac{1}{2})\hbar\Omega_s, \quad (2.14')$$

$$\mathcal{H}'=i(\hbar D^2/2MN)^{\frac{1}{2}}\sum_s\sum_{q,q'}\sum_{\mathbf{f}}\frac{fF_s}{\Omega_s{}^{\frac{1}{2}}} \times[(q'|e^{i\mathbf{f}\cdot\mathbf{r}}|q)b_{\mathbf{f}}{}^{(s)}-(q'|e^{-i\mathbf{f}\cdot\mathbf{r}}|q)b_{\mathbf{f}}{}^{(s)*}]a_{q'}{}^* a_q \equiv\sum_s\sum_{q,q'}(q'|\delta V_s|q)a_{q'}{}^* a_q. \quad (2.14'')$$

The matrix elements $(q'|e^{\pm i\mathbf{f}\cdot\mathbf{r}}|q)$ are given by

$$(q'|e^{i\mathbf{f}\cdot\mathbf{r}}|q)=\delta_{\kappa',\kappa+\eta}J_{q',q}(f_x), \quad (q'|e^{-i\mathbf{f}\cdot\mathbf{r}}|q)=\delta_{\kappa',\kappa-\eta}J_{q',q}(-f_x), \quad (2.15)$$

where κ and η are two dimensional wave vectors with components k_y, k_z and f_y, f_z, and $J_{q',q}(\pm f_x)$ has the property

$$J_{q',q}(-f_x{}^*) =\int_{-\infty}^{\infty}\exp\{i[Q(x-x_0')-Q(x-x_0)+f_x x]\} \times\phi_{n'}(x-x_0')\phi_n(x-x_0)dx =J_{q,q'}(f_x). \quad (2.16)$$

By using this, we obtain

$$(q|\delta V_s|q')(q'|\delta V_s|q) =(\hbar D^2/2MN)\sum_{\mathbf{f}}\frac{f^2F_s{}^2}{\Omega_s}\delta_{\kappa',\kappa-\eta}|J_{q',q}(-f_x)|^2 \times(b_{\mathbf{f}}{}^{(s)*}b_{\mathbf{f}}{}^{(s)}+1), \quad (2.17)$$

for the emission of a phonon and

$$(q|\delta V_s|q')(q'|\delta V_s|q) =(\hbar D^2/2MN)\sum_{\mathbf{f}}\frac{f^2F_s{}^2}{\Omega_s}\delta_{\kappa',\kappa+\eta}|J_{q',q}(f_x)|^2 b_{\mathbf{f}}{}^{(s)*}b_{\mathbf{f}}, \quad (2.18)$$

for the absorption of a phonon.

We shall give an explicit expression for $|J_{q',q}(f_x)|^2$.

$$Q(x-x_0')-Q(x-x_0) =-\left[\frac{\alpha_{xy}}{\alpha_{xx}}(k_y'-k_y)+\frac{\alpha_{zz}}{\alpha_{xx}}(k_z'-k_z)\right]x-\nu_{q'q},$$

where $\nu_{q'q}$ is a function independent of x and $\nu_{q'q}=-\nu_{qq'}$. Then

$$J_{q',q}(f_x) =e^{i\nu_{q'q}}\int\exp\left[i\left(f_x+\frac{\alpha_{xy}}{\alpha_{xx}}f_y+\frac{\alpha_{zz}}{\alpha_{xx}}f_z\right)x\right] \times\phi_{n'}(x-x_0')\phi_n(x-x_0)dx =e^{i\nu_{q'q}}\int\exp[i\alpha_{xx}{}^{-\frac{1}{2}}f_x' x]\phi_{n'}(x-x_0')\phi_n(x-x_0)dx =e^{i\nu_{q'q}}\int\exp[i\xi s)\Phi_n(s-s_0')\Phi_n(s-s_0)ds. \quad (2.19)$$

In the above expression the following variables were introduced:

$$f_x'=\alpha_{xx}{}^{\frac{1}{2}}\left(f_x+\frac{\alpha_{xy}}{\alpha_{xx}}f_y+\frac{\alpha_{zz}}{\alpha_{xx}}f_z\right),$$

$$f_y'=\alpha_{xx}{}^{-\frac{1}{2}}[\omega(z)/\omega_0]\left[f_y+\frac{\alpha_{xx}\alpha_{yz}-\alpha_{xy}\alpha_{zz}}{[\omega(z)/\omega_0]^2}f_z\right] =-g(m\omega(z)/\hbar)^{\frac{1}{2}}(s_0'-s_0), \quad (2.20)$$

$$f_z'=\lambda_z{}^{\frac{1}{2}}f_z,$$

and

$$\xi=[m\omega(z)/h]^{-\frac{1}{2}}f_{x'},\qquad(2.21)$$
$$\zeta=[m\omega(z)/h]^{-\frac{1}{2}}f_{y'},$$

from which it is easily shown that

$$\mathbf{f}\cdot\boldsymbol{\alpha}\cdot\mathbf{f}=f'^2.\qquad(2.22)$$

Equation (2.19) is just the same as Titeica's expression.[7] Thus, we can use his result for $|J_{q',q}(f_x)|^2$ with the substitution for his $\mathbf{f}$ and ω_0 by $\mathbf{f}'$ and $\omega(z)$. An explicit expression for $|J_{q',q}(f_x)|^2$ in the region $n, n'\gg1$ is given by

$$|J_{q',q}(f_x)|^2=(1/\pi)[(n+n'+1)\delta^2-(n-n')^2-\tfrac{1}{4}\delta^4]^{-\frac{1}{2}},$$
$$\delta^2=\xi^2+\zeta^2.\qquad(2.23)$$

III. CONDUCTIVITY TENSOR

Before starting the calculation of the conductivity tensor, we give the matrix element of p_x and x, and then the current density operators. These can be easily calculated by using the wave function (2.3). The result is

$$\begin{aligned}
&(q|p_x|q)=(\alpha_{xy}\alpha_{yz}-\alpha_{yy}\alpha_{zx})[\omega(z)/\omega_0]^{-2}\hbar k_z,\\
&(q|p_x|q')=\alpha_{xx}^{-\frac{1}{2}}[m\hbar\omega(z)]^{\frac{1}{2}}2^{-\frac{1}{2}}\\
&\qquad\times\{\mp i-g\alpha_{xy}[\omega(z)/\omega_0]^{-1}\}\\
&\qquad\times[(n+1)^{\frac{1}{2}}\delta_{n',n+1}+n^{\frac{1}{2}}\delta_{n',n-1}]\delta_{\kappa,\kappa'},\qquad(3.1)\\
&(q|x|q)=x_0,\\
&(q|x|q')=\alpha_{xx}^{\frac{1}{2}}[m\omega(z)/\hbar]^{-\frac{1}{2}}\\
&\qquad\times2^{-\frac{1}{2}}[(n+1)^{\frac{1}{2}}\delta_{n',n+1}+n^{\frac{1}{2}}\delta_{n',n-1}]\delta_{\kappa,\kappa'}.
\end{aligned}$$

The current density operators are given by

$$\begin{pmatrix}j_x\\j_y\\j_z\end{pmatrix}=\begin{pmatrix}\alpha_{xx}&\alpha_{xy}&0\\\alpha_{xy}&\alpha_{yy}&0\\\alpha_{zx}&\alpha_{yz}&\lambda_z\end{pmatrix}\times\begin{pmatrix}A(x)\\B(x)\\C(z)\end{pmatrix},\qquad(3.2)$$

where

$$A(x)=-(g|e|/m)\sum_{q\neq q'}(q|p_x|q')a_q^*a_{q'},$$
$$B(x)=-(g|e|/m)gm\omega_0\sum_{q\neq q'}(q|x|q')a_q^*a_{q'},$$
$$C(z)=-(g|e|/m)\sum_q\hbar k_z a_q^*a_q.$$

The schemes of the calculations for the transverse and the longitudinal components are different, and these are given in separate paragraphs.

A. Transverse Tensor

The electric field is assumed to be parallel to the x axis. By this arrangement we can get the components $\sigma_{xx}(z)$, $\sigma_{yx}(z)$, and $\sigma_{zx}(z)$.

$$\begin{aligned}
J_x^l(z)&=\mathrm{Tr}(\rho^l j_x^l)\\
&=2\sum_{n,\kappa}[\rho_{n\kappa,(n-1)\kappa}{}^l j_x{}^l(n-1,n)\\
&\qquad+\rho_{n\kappa,(n+1)\kappa}{}^l j_x{}^l(n+1,n)].\qquad(3.3)
\end{aligned}$$

[7] S. Titeica, Ann. Physik **22**, 129 (1935).

The real part of the matrix element $j_x(n\pm1,n)$ originating from the nonvanishing $\alpha_{xy}{}^l$ is canceled, and we get

$$\begin{aligned}
J_x^l(z)&=-i2g_l|e|\alpha_{xx}{}^l[\hbar\omega_l(z)/m]^{\frac{1}{2}}\\
&\quad\times2^{-\frac{1}{2}}\textstyle\sum_{n,\kappa}[\rho_{n\kappa,(n+1)\kappa}{}^l(n+1)^{\frac{1}{2}}-\rho_{n\kappa,(n-1)\kappa}{}^l n^{\frac{1}{2}}]\\
&\equiv\sigma_{xx}{}^l(z)F_x.\qquad(3.4)
\end{aligned}$$

On the other hand, $J_y^l(z)$ has two parts,

$$\begin{aligned}
J_y^l(z)&=-i2g_l|e|\alpha_{xy}{}^l\alpha_{xx}{}^{l-\frac{1}{2}}[\omega_l(z)/\omega_0]^{\frac{1}{2}}(\hbar\omega_0/m)^{\frac{1}{2}}\\
&\quad\times2^{-\frac{1}{2}}\sum_{n,\kappa}[\rho_{n\kappa,(n+1)\kappa}{}^l(n+1)^{\frac{1}{2}}-\rho_{n\kappa,(n-1)\kappa}{}^l n^{\frac{1}{2}}]\\
&\quad-2|e|\alpha_{xx}{}^{l-\frac{1}{2}}[\omega_l(z)/\omega_0]^{\frac{1}{2}}(\hbar\omega_0/m)^{\frac{1}{2}}\\
&\quad\times2^{-\frac{1}{2}}\sum_{n,\kappa}[\rho_{n\kappa,(n+1)\kappa}{}^l(n+1)^{\frac{1}{2}}+\rho_{n\kappa,(n-1)\kappa}{}^l n^{\frac{1}{2}}]\\
&\equiv\sigma_{yx}{}^{ls}(z)F_x+\sigma_{yx}{}^{la}(z)F_x.\qquad(3.5)
\end{aligned}$$

The first term of $J_y^l(z)$ is equal to $(\alpha_{xy}{}^l/\alpha_{xx}{}^l)\sigma_{xx}{}^l(z)F_x$ and this is the symmetric part of $J_y^l(z)$. Similarly,

$$\begin{aligned}
J_z^l(z)&=-i2g_l|e|\alpha_{zx}{}^l\alpha_{xx}{}^{l-\frac{1}{2}}[\omega_l(z)/\omega_0]^{\frac{1}{2}}(\hbar\omega_0/m)^{\frac{1}{2}}\\
&\quad\times2^{-\frac{1}{2}}\sum_{n,\kappa}[\rho_{n\kappa,(n+1)\kappa}{}^l(n+1)^{\frac{1}{2}}-\rho_{n\kappa,(n-1)\kappa}{}^l n^{\frac{1}{2}}]\\
&\quad-2|e|\alpha_{xx}{}^{l-\frac{1}{2}}(\alpha_{xx}{}^l\alpha_{yz}{}^l-\alpha_{xy}{}^l\alpha_{zx}{}^l)[\omega_l(z)/\omega_0]^{-\frac{1}{2}}\\
&\quad\times(\hbar\omega_0/m)^{\frac{1}{2}}2^{-\frac{1}{2}}\sum_{n,\kappa}[\rho_{n\kappa,(n+1)\kappa}{}^l(n+1)^{\frac{1}{2}}\\
&\quad+\rho_{n\kappa,(n-1)\kappa}{}^l n^{\frac{1}{2}}]\\
&\equiv\sigma_{zx}{}^{ls}(z)F_x+\sigma_{zx}{}^{la}(z)F_x.\qquad(3.6)
\end{aligned}$$

Thus the symmetric parts are expressed as

$$\sigma_{xx}{}^l(z),\ \sigma_{yx}{}^{ls}(z)=\frac{\alpha_{xy}{}^l}{\alpha_{xx}{}^l}\sigma_{xx}{}^l(z),\ \sigma_{zx}{}^{ls}(z)=\frac{\alpha_{zx}{}^l}{\alpha_{xx}{}^l}\sigma_{xx}{}^l(z).\qquad(3.7)$$

Secondly, we assume the electric field parallel to the y axis. In this case we can get the components $\sigma_{yy}{}^l(z)$, $\sigma_{xy}{}^l(z)$, and $\sigma_{zy}{}^l(z)$. The relation among the symmetric parts is quite similar to (3.7), i.e.,

$$\sigma_{yy}{}^l(z),\ \sigma_{xy}{}^{ls}(z)=\frac{\alpha_{xy}{}^l}{\alpha_{yy}{}^l}\sigma_{yy}{}^l(z),\ \sigma_{zy}{}^{ls}(z)=\frac{\alpha_{yz}{}^l}{\alpha_{yy}{}^l}\sigma_{yy}{}^l(z).\qquad(3.8)$$

From symmetry it must be that

$$\sigma_{yx}{}^{ls}(z)=\sigma_{xy}{}^{ls}(z).$$

Then we obtain the relation

$$\sigma_{ij}{}^{ls}(z)/\alpha_{ij}{}^l=\sigma_{xx}{}^l(z)/\alpha_{xx}{}^l\quad(\text{except } i=j=z),\qquad(3.9)$$

i.e., we can get all transverse symmetric parts from the calculation of only $\sigma_{xx}{}^l(z)$ in a fixed direction of magnetic field.

First, we give an explicit expression for the anti-

symmetric part of σ_{ij}. The density matrix $\rho_{n,n'}$ is expanded in power series of the perturbing potential,

$$\rho_{n,n'}{}^{l}=\rho_{n,n'}{}^{l(0)}+\rho_{n,n'}{}^{l(1)}+\rho_{n,n'}{}^{l(2)}+\cdots. \quad (3.10)$$

Argyres and Roth[8] have given a formula for $\rho_{n,n'}{}^{(s)}$ and $\rho_{n,n'}{}^{l(0)}$:

$$\rho_{n,n'}{}^{l(0)}=[f(\epsilon_n{}^{l})-f(\epsilon_{n'}{}^{l})/(\epsilon_n{}^{l}-\epsilon_{n'}{}^{l})] \times g_l|e|F_x(n|x|n'). \quad (3.11)$$

This zero-order term gives a nonvanishing contribution to the antisymmetric part,

$$\begin{aligned}\sigma_{yx}{}^{la}(z)&=(-g_le^2/m\omega_0)\\ &\sum_{n,\kappa}[-(n+1)(f_n-f_{n+1})+n(f_n-f_{n-1})] \quad (3.12)\\ &=(g_le^2/m\omega_0)2\textstyle\sum_{n,\kappa}f_n\\ &=(g_le^2/m\omega_0)n_l.\end{aligned}$$

Similarly, we get

$$\sigma_{zx}{}^{la}(z)=g_l\frac{n_le^2}{m\omega_0}\frac{\alpha_{xx}{}^{l}\alpha_{yz}{}^{l}-\alpha_{xy}{}^{l}\alpha_{zx}{}^{l}}{[\omega_l(z)/\omega_0]^2}. \quad (3.13)$$

Secondly, we calculate the symmetric part of σ_{ij}. As was shown, it is sufficient to calculate $\sigma_{xx}{}^{l}(z)$. A real $\rho_{n,n'}{}^{l(0)}$ does not contribute to $\sigma_{xx}{}^{l}(z)$. By using Argyres and Roth's expression for $\rho_{n,n'}{}^{(2)}$ and (3.4), we can see that our $\sigma_{xx}{}^{l}(z)$ is different from theirs only in that their ω_0 is replaced by $\omega_l(z)$ and $\alpha_{xx}{}^{l\frac{1}{2}}$ is multiplied by a factor. However, the resultant factor $\alpha_{xx}{}^{l\frac{1}{2}}\times[\omega_l(z)/\omega_0]^{-\frac{1}{2}}$ is canceled in rewriting the product $[2^{\frac{1}{2}}(n+1)^{\frac{1}{2}}V_{n,n'}V_{n',n+1}+(2n)^{\frac{1}{2}}V_{n+1,n'}V_{n',n}]$ in terms of the difference of center coordinates, i.e., of $\alpha_{xx}{}^{l-\frac{1}{2}}\times[\omega_l(z)/\omega_0]^{\frac{1}{2}}(x_0-x_0')$, by using the property of the harmonic oscillator functions. The additional phase factor $\exp(iQ)$ does not give rise to any essential change in their derivation of Titeica's expression for the conductivity.

Thus we obtain

$$\begin{aligned}\sigma_{xx}{}^{l}(z)=(e^2/kT)\sum_{s}\sum_{q,q'}&f_{q'}(1-f_{q'})(x_0-x_0')^2\\ &\times[(2\pi/\hbar)(\hbar D^2/2MN)\sum_{\mathbf{f}}(f^2/\Omega_s)F_s{}^2\\ &\times\{|J_{q',q}(f_x)|^2N_{\mathbf{f}}{}^{(s)}\delta_{\kappa',\kappa+\eta}\delta(\epsilon_{q'}-\epsilon_q-\hbar\Omega_s)\\ &+|J_{q',q}(-f_x)|^2(N_{\mathbf{f}}{}^{(s)}+1)\\ &\times\delta_{\kappa',\kappa-\eta}\delta(\epsilon_{q'}-\epsilon_q+\hbar\Omega_s)\}]. \quad (3.14)\end{aligned}$$

Summations over q', q, and $\mathbf{f}$ are replaced by integrations,

$$\begin{aligned}\sum_{q,q'}\sum_{\mathbf{f}}A&=2^2(1/2\pi)^5(m\omega_0/\hbar)^2\\ &\times\sum_{n}\sum_{n'}\int A\,dk_z\,dk_z'\,dx_0\,dx_0'\,df_x. \quad (3.15)\end{aligned}$$

Changing the variables

$$\begin{aligned}X&=x_0+x_0', \quad K=k_z+k_z',\\ X'&=x_0-x_0', \quad K'=k_z-k_z',\end{aligned}$$

converts Eq. (3.15) to

$$\begin{aligned}\sum_{q,q'}\sum_{\mathbf{f}}A&=(1/2\pi)^5(m\omega_0/\hbar)\\ &\times\sum_{n,n'}\int A\,df_x\,df_y\,df_z\,dK\,dX. \quad (3.15')\end{aligned}$$

The argument of the δ function may be written as

$$\epsilon_{q'}-\epsilon_q\mp\hbar\Omega_s=\hbar\omega_l(z)(n'-n)-\tfrac{1}{2}\lambda_z{}^{l}\hbar^2KK'/m\mp\hbar\Omega_s.$$

Then we integrate first over K. Using the selection rules and well-known properties of Fermi and Bose functions, we obtain for $\sigma_{xx}{}^{l}(z)$,

$$\begin{aligned}\sigma_{xx}{}^{l}(z)=&\frac{e^2(D^2/MN)(1/kT)}{2^4\pi^4\hbar\omega_0\lambda_z{}^{l}[\omega_l(z)/\omega_0]^2}\\ &\times\sum_{s}\sum_{n,n'}\int d\mathbf{f}\frac{f^2F_s{}^2}{|f_z|\Omega_s}f_y{}'^2W_{n',n}(\xi^2+\zeta^2)\\ &\times N_{\mathbf{f}}{}^{(s)}(N_{\mathbf{f}}{}^{(s)}+1)[(f_q-f_{q'})_{\rm abs}+(f_{q'}-f_q)_{\rm emis}], \quad (3.16)\end{aligned}$$

where

$$W_{n',n}(\xi^2+\zeta^2)=|J_{q',q}(f_x)|^2{}_{\kappa'=\kappa+\eta}=|J_{q',q}(-f_x)|^2{}_{\kappa'=\kappa-\eta}.$$

Now we perform the summation over n and n'. We can follow Titeica's calculation except that $\mathbf{f}$ and ω_0 are replaced by $\mathbf{f}'$ and $\omega_l(z)$ in ours. Using the step function as an approximation for the Fermi function, the result is

$$\begin{aligned}\sum_{n,n'}W_{n',n}(\xi^2+\zeta^2)&[(f_q-f_{q'})_{\rm abs}+[f_{q'}-f_q)_{\rm emis}]\\ &\sim 2x[kT/\hbar\omega_l(z)](|f_z'|/f'). \quad (3.17)\end{aligned}$$

Thus

$$\begin{aligned}\sigma_{xx}{}^{l}(z)=&\frac{\alpha_{xx}{}^{l}e^2(D^2/MN)(kT)^5}{8\pi^4\hbar^7\omega_l(z)^2(\det\boldsymbol{\alpha}^{l})^{\frac{1}{2}}}\sum_{s}\frac{1}{v_s}\int_0^{x_s{}^{l}}dx\int_0^{2\pi}d\varphi\int_0^{\pi}d\theta\\ &\times\frac{x^5e^x(f_y'/f)^2F_s{}^2}{(e^x-1)^2(f'/f)}\sin\theta, \quad (3.18)\end{aligned}$$

where

$$x_s{}^{l}=h\nu_m/kT=2^{\frac{1}{2}}\zeta_l{}^{\frac{1}{2}}(m^*v_s{}^2)^{\frac{1}{2}}/kT, \quad (3.19)$$

or $x_s{}^{l}$ is rewritten as

$$x_s{}^{l}=(2\zeta_l/E_0{}^{l})^{\frac{1}{2}}(\Theta_s/T), \quad (3.19')$$

with

$$E_0{}^{l}=(\hbar^2/2m_l{}^*a^2)(3\pi^2/\sqrt{2})^{\frac{2}{3}},$$

where ζ_l is the Fermi energy of lth band and $m_l{}^*=(\det\boldsymbol{\alpha}^{l})^{-\frac{1}{3}}m$ and a is the atomic distance. The limitation (3.19) arises from the fact that in semimetals the

electrons can interact only with very long lattice waves.[9] If we consider metals, we should put $x_s{}^l=\Theta_s/T$, as Titeica did. $E_0{}^l$ is the same order of magnitude as the Fermi energy in metals so that for semimetals $x_s{}^l$ is much smaller than Θ_s/T. In other words, we can treat the lattice scattering as elastic down to temperatures much lower than the Debye temperature.

We rewrite (3.18) as

$$\sigma_{xx}(z)=\sum_l(\alpha_{xx}{}^l n_l e^2/m\omega_l(z)^2)[\tau^l(z)^{-1}], \quad (3.20)$$

where

$$[\tau^l(z)^{-1}]=\frac{m(D^2/MN)(kT)^5}{8\pi^4\hbar^7 n_l(\det\boldsymbol{\alpha}^l)^{\frac{1}{3}}}\sum_s\frac{1}{v_s{}^6}\int_0^{x_s{}^l}\frac{x^5e^x dx}{(e^x-1)^2}$$
$$\times\int_0^{2\pi}d\varphi\int_0^{\pi}d\theta\frac{F_s{}^2\sin\theta(f_y'/f)^2}{(f'/f)}. \quad (3.21)$$

By changing the variables f, θ, φ into f', Θ, Φ, i.e., by considering $\partial(f,\theta,\varphi)/\partial(f',\Theta,\Phi)=(\det\boldsymbol{\alpha}^l)^{\frac{1}{3}}$, we can write

$$[\tau^l(z)^{-1}]=\frac{m(D^2/MN)(kT)^5}{8\pi^4\hbar^7 n_l(\det\boldsymbol{\alpha}^l)}\sum_s\frac{1}{v_s{}^6}\int_0^{x_s{}^{l\prime}}dx'$$
$$\times\int_0^{2\pi}d\Phi\int_0^{\pi}d\Theta\frac{x'^5e^{x'f/f'}(f/f')^2(f_y'/f')^2}{(e^{x'f/f'}-1)^2}$$
$$\times F_s{}^2(\Theta,\Phi)\sin\Theta, \quad (3.22)$$

where

$$x_s'=(m_l*/m)^{-\frac{1}{2}}x_s{}^l.$$

This expression (3.22) is not easily integrable. However, for the case of an isotropic deformation potential and in the high-temperature region where

$$F_1=1, \quad F_2=F_3=0, \quad e^x\sim 1+x, \quad (3.23)$$

we obtain

$$[\tau^l(z)^{-1}]=\frac{m(D^2/MN)(kT)^5 x_1{}^{l4}}{24\pi^3\hbar^7 n_l(\det\boldsymbol{\alpha}^l)^{\frac{1}{3}}v_1{}^6}$$
$$=3\pi(D^2/N\hbar)(kT/Mv_1{}^2)(n_l/\zeta_l). \quad (3.24)$$

This suggests the following approximate substitution in Eq. (3.21)

$$(f_y'/f')^2(f'/f)\rightarrow\tfrac{1}{2}(\det\boldsymbol{\alpha}^l)^{1/6}(f_x{}^2+f_y{}^2/f^2), \quad (3.25)$$

by which we can also obtain the same result (3.24) for the same case (3.23). Thus (3.21) is rewritten as

$$[\tau^l(z)^{-1}]=\frac{m(D^2/MN)(kT)^5}{8\pi^4\hbar^7 n_l(\det\boldsymbol{\alpha}^l)^{\frac{1}{3}}}\sum_s\frac{1}{v_s{}^6}\int_0^{x_s{}^l}dx$$
$$\times\frac{x^5e^x}{(e^x-1)^2}\int_0^{2\pi}d\varphi\int_0^{\pi}d\theta\,F_s{}^2\sin\theta$$
$$\times(f_x{}^2+f_y{}^2)/2f^2. \quad (3.26)$$

[8] P. N. Argyres and L. M. Roth, J. Phys. Chem. Solids **12**, 89 (1959); see also P. N. Argyres, Phys. Rev. **117**, 315 (1960).
[9] E. H. Sondheimer, Proc. Phys. Soc. (London) **A65**, 561 (1952).

B. Longitudinal Tensor

Both the electric and magnetic fields are assumed to be along the z axis. The current density is

$$J_z{}^l(z)=\mathrm{Tr}(\rho^l j_z{}^l)$$
$$=\sum_{n,\kappa}\rho_{n\kappa,n\kappa}{}^l j_z{}^l(n,n)+2\sum_{n,\kappa}[\rho_{n\kappa,(n-1)\kappa}{}^l j_z{}^l(n-1,n)$$
$$+\rho_{n\kappa,(n+1)\kappa}{}^l j_z{}^l(n+1,n)]. \quad (3.27)$$

The nondiagonal components $\rho_{n\kappa,(n\pm1)\kappa}$ are smaller than $\rho_{n\kappa,n\kappa}$ in the order of V, as can be seen from the structure of the equation of motion for ρ. Then we look for explicit expressions for the diagonal terms $\rho_{n\kappa,n\kappa}$ using the stationary equation

$$d\rho_q/dt=(i/\hbar)C_{q,q}{}^{(0)}$$
$$+\sum_{q'}[W_{q,q'}\rho_{q'}(1-\rho_q)-W_{q',q}\rho_q(1-\rho_{q'})]=0, \quad (3.28)$$

where

$$C_{q,q}{}^{(0)}=g|e|E_z(\hbar/i)(\lambda_z\hbar k_z/m)f'(\epsilon_q),$$
$$W_{q,q'}=(2\pi/\hbar)(\hbar D^2/2MN)\sum_s\sum_{\mathrm{f}}f^2F_s{}^2/\Omega_s$$
$$\times[\delta_{\kappa,\kappa'-\eta}|J_{q,q'}(-f_x)|^2(N_{\mathrm{f}}{}^{(s)}+1)$$
$$\times\delta(\epsilon_q-\epsilon_{q'}+\hbar\Omega_s)+\delta_{\kappa,\kappa'+\eta}|J_{q,q'}(f_x)|^2$$
$$\times N_f{}^{(s)}\delta(\epsilon_q-\epsilon_{q'}-\hbar\Omega_s)]. \quad (3.29)$$

The following type of solution for $\rho_q{}^l$ is assumed:

$$\rho_q{}^l=f_n+(\lambda_z{}^l\hbar^2k_z/mkT)f_n(1-f_n)\bar{K}_l, \quad (3.30)$$

where $\bar{K}_l$ is a constant with the dimension of wave number. We put this into (3.28), multiply by k_z, and sum up over q. The procedure for the calculation is quite similar to that of $\sigma_{xx}{}^l(z)$, and we can use most of those results. Thus, we obtain

$$g_l|e|E_z n_l/\hbar+n_l\{\tau^l(z)^{-1}\}\bar{K}_l=0, \quad (3.31)$$

where $\{\tau^l(z)^{-1}\}$ is the same as $[\tau^l(z)^{-1}]$ except that $(f_z'/f)^2$ appears instead of $(f_y'/f)^2$ in (3.21). This $(f_z'/f)^2/(f'/f)$ is replaced by $(\det\boldsymbol{\alpha}^l)^{1/6}(f_z/f)^2$ as in (3.25). Then we can easily get the result

$$\sigma_{zz}(z)=\sum_l\lambda_z{}^l n_l e^2/m\{\tau^l(z)^{-1}\}. \quad (3.32)$$

C. Representation of All Tensor Components

The other components of the conductivity tensor are obtained by cyclic permutations of the following:

$$\sigma_{ij}{}^a(k)=-\sum_l(g_l n_l e^2/m\omega_0)$$
$$(i,j,k \text{ are cyclic over } x,y,z),$$
$$\sigma_{ik}{}^a(k)=-\sum_l(g_l n_l e^2/m\omega_0)\frac{\alpha_{ik}{}^l\alpha_{ji}{}^l-\alpha_{ii}{}^l\alpha_{kj}{}^l}{[\omega_l(k)/\omega_0]^2} \quad (3.33)$$
$$(i,k,j \text{ are cyclic over } x,y,z).$$

Components of the type $\sigma_{kj}{}^a(k)$ are obtained by merely interchanging i and j in $\sigma_{ik}{}^a(k)$ because of the

double reversal of sign on the lettering $i \rightleftarrows j$ and $\sigma_{jk}{}^{a}(k) = -\sigma_{kj}{}^{a}(k)$. In this case, however, k, j, i are cyclic over x, y, z; n_l is approximated by its value in the absence of a magnetic field.

On the other hand, the symmetric parts are expressed by the following:

$$\sigma_{ij}{}^{s}(k) = \sum_l [\lambda_k{}^l n_l e^2/m\{\tau^l(k)^{-1}\}]\delta_{ij}\delta_{jk} + \sum_l \alpha_{ij}{}^l n_l e^2 [\tau^l(k)^{-1}]/m\omega_l(k)^2, \quad (3.34)$$

where

$$\{\tau^l(k)^{-1}\} = 3\pi(D^2/N\hbar)(kT/Mv_1^2)(n_l/\zeta_l) \times \sum_s (v_s/v_1)^{-2} J_s{}^l(T)\{G_s{}^l(k)\}, \quad (3.35)$$

$$[\tau^l(k)^{-1}] = 3\pi(D^2/N\hbar)(kT/Mv_1^2)(n_l/\zeta_l) \times \sum_s (v_s/v_1)^{-2} J_s{}^l(T)[G_s{}^l(k)], \quad (3.36)$$

with

$$J_s{}^l(T) = \frac{4}{x_s{}^{l4}} \int_0^{x_s{}^l} dx \frac{x^5 e^x}{(e^x-1)^2}, \qquad x_s{}^l = 2^{\frac{1}{2}} \zeta_l{}^{\frac{1}{2}} (m_l{}^* v_s^2)^{\frac{1}{2}}/kT, \quad (3.37)$$

$$\{G_s{}^l(k)\} = (1/2\pi)(3/4\pi) \int_0^{2\pi} d\chi \int_0^{2\pi} d\varphi \int_0^{\pi} d\theta \times \sin\theta F_s{}^2(\theta,\varphi)(f_\kappa{}^2/f^2), \quad (3.38)$$

$$[G_s{}^l(k)] = (1/2\pi)(3/4\pi) \int_0^{2\pi} d\chi \int_0^{2\pi} d\varphi \int_0^{\pi} d\theta \times \sin\theta F_s{}^2(\theta,\varphi)(f_m{}^2+f_n{}^2)/2f^2, \quad (3.39)$$

where m, n, k should by cyclic over x, y, z. Explicit expressions for $\{G_s(k)\}$ and $[G_s{}^l(k)]$ are

$$\{G_1{}^l(k)\} = (1/35)[3(c_{mm}{}^{l2}+c_{nn}{}^{l2})+15c_{\kappa\kappa}{}^{l2} +2c_{mm}{}^l c_{nn}{}^l+6(c_{mm}{}^l+c_{nn}{}^l)c_{\kappa\kappa}{}^l+4c_{mn}{}^{l2} +12(c_{n\kappa}{}^{l2}+c_{\kappa m}{}^{l2})], \quad (3.40$$

$$\{G_2{}^l(k)\} = (1/35)[2(c_{mm}{}^{l2}+c_{nn}{}^{l2})+3c_{\kappa\kappa}{}^{l2} -c_{mm}{}^l c_{nn}{}^l-3(c_{mm}{}^l+c_{nn}{}^l)c_{\kappa\kappa}{}^l+5c_{mn}{}^{l2} +8(c_{n\kappa}{}^{l2}+c_{\kappa m}{}^{l2})], \quad (3.41)$$

$$[G_1{}^l(k)] = (1/35)[9(c_{mm}{}^{l2}+c_{nn}{}^{l2})+3c_{\kappa\kappa}{}^{l2} +6c_{mm}{}^l c_{nn}{}^l+4(c_{mm}{}^l+c_{nn}{}^l)c_{\kappa\kappa}{}^l+12c_{mn}{}^{l2} +8(c_{n\kappa}{}^{l2}+c_{\kappa m}{}^{l2})], \quad (3.42)$$

$$[G_2{}^l(k)] = (1/35)[(5/2)(c_{mm}{}^{l2}+c_{nn}{}^{l2})+2c_{\kappa\kappa}{}^{l2} -3c_{mm}{}^l c_{nn}{}^l-2(c_{mm}{}^l+c_{nn}{}^l)c_{\kappa\kappa}{}^l+8c_{mn}{}^{l2} +(13/2)(c_{n\kappa}{}^{l2}+c_{\kappa m}{}^{l2})]. \quad (3.43)$$

In the case of an isotropic deformation potential, i.e., in the case of $c_{ii}=1$, $c_{ij}=0$ $(i \neq j)$, we obtain

$$\{G_1{}^l(k)\} = [G_1{}^l(k)] = 1, \qquad \{G_2{}^l(k)\} = [G_2{}^l(k)] = 0. \quad (3.44)$$

In other words, the transverse phonons do not interact with electrons as expected. Further, if we limit ourselves to the high-temperature region such that $x_s{}^l \lesssim 0.5$, we should put

$$J_s{}^l(T) = 1. \quad (3.45)$$

In the case of bismuth (3.45) is approximately satisfied even down to 10°K.

IV. CONDUCTIVITY TENSOR IN INTERMEDIATE MAGNETIC FIELDS

The conductivity expressions given in the previous section are the classical limit for the high-magnetic-field region $\omega_c\tau \gg 1$, in which quantum effects are neglected. In order to explain the characteristics of our experimental curves of the antisymmetric part of the resistivity tensor, it is very important to take account of the deviation from the high-magnetic-field limit (3.33) and (3.34). Presenting the conductivity expression for intermediate magnetic fields thus has practical meaning.

We cannot, unfortunately, develop an exact theory applicable in the intermediate region for anisotropic scattering. However, it is possible to write down an interpolation formula for this case. For intermediate fields, the conductivity tensor components should have the following form:

$$\sigma_{ij}(\mathbf{H}) = \sum_l \left\{ \frac{n_l e_l c}{H_i}[\omega_l(H_i)\tau^l(H_i)]^2 \frac{\alpha_{ij}{}^l\alpha_{jk}{}^l - \alpha_{jj}{}^l\alpha_{ki}{}^l}{\alpha_{jj}{}^l\alpha_{kk}{}^l - \alpha_{jk}{}^{l2}} + \frac{n_l e_l c}{H_j}[\omega_l(H_j)\tau^l(H_j)]^2 \frac{\alpha_{ij}{}^l\alpha_{ki}{}^l - \alpha_{ii}{}^l\alpha_{jk}{}^l}{\alpha_{kk}{}^l\alpha_{ii}{}^l - \alpha_{ki}{}^{l2}} + \frac{n_l e_l c}{H_k}[\omega_l(H_k)\tau^l(H_k)]^2 \right\} \frac{1}{1+[\omega_l(\mathbf{H})\tau^l(\mathbf{H})]^2} + \sum_l \{\alpha_{ij}{}^l n_l e^2 \tau^l(\mathbf{H})/m + [\lambda^l(i)\lambda^l(j)]^{\frac{1}{2}} n_l e^2 \langle\tau^l(\mathbf{H})\rangle/m \times \omega_l(H_i)\tau^l(H_i)\omega_l(H_j)\tau^l(H_j)\} \frac{1}{1+[\omega_l(\mathbf{H})\tau^l(\mathbf{H})]^2}, \quad (4.1)$$

where $\omega_l(\mathbf{H})$ is the cyclotron frequency in a magnetic field $\mathbf{H}$ and

$$\tau^l(\mathbf{H}) = [\tau^l(\mathbf{H})^{-1}]^{-1}, \quad (4.2)'$$

$$\langle\tau^l(\mathbf{H})\rangle = \{\tau^l(\mathbf{H})^{-1}\}^{-1}. \quad (4.2)''$$

$[\tau^l(\mathbf{H})^{-1}]$ and $\{\tau^l(\mathbf{H})^{-1}\}$ have structures similar to those of $[\tau^l(k)^{-1}]$ and $\{\tau^l(k)^{-1}\}$. But instead of $[G_s{}^l(k)]$ and $\{G_s{}^l(k)\}$, $[G_s{}^l(\mathbf{H})]$ and $\{G_s{}^l(\mathbf{H})\}$ enter in (4.2)′ and (4.2)″, respectively.

$$\{G_s{}^l(\mathbf{H})\} = (1/2\pi)(3/4\pi) \int_0^{2\pi} d\chi \int_0^{2\pi} d\varphi \int_0^{\pi} d\theta \times F_s{}^2 \sin\theta (f_{11}/f)^2, \quad (4.3)$$

$$[G_s^l(\mathbf{H})]=(1/2\pi)^2(3/4\pi)\int_0^{2\pi}d\psi\int_0^{2\pi}d\chi\int_0^{2\pi}d\varphi\int_0^{\pi}d\theta \times F_s^2\sin\theta(f_\perp/f)^2, \quad (4.4)$$

where $f_{\parallel}$ and $f_\perp$ are given by

$$f_{\parallel}/f=(f_x/f)\sin\Theta\cos\Phi+(f_y/f)\sin\Theta\sin\Phi+(f_z/f)\cos\Theta,$$

$$f_\perp/f=(f_x/f)(-\cos\psi\cos\Theta\cos\Phi+\sin\psi\sin\Phi)+(f_y/f)(-\cos\psi\cos\Theta\sin\Phi-\sin\psi\cos\Phi)+(f_z/f)\cos\psi\sin\Theta.$$

Θ and Φ specify the direction of the magnetic field, and ψ specifies the direction perpendicular to the magnetic field. Then Θ, Φ, and ψ correspond to θ, φ, and χ in Fig. 1.

The contribution from the quadratic term $(f_i/f)^2$ was already given in (3.38). The remaining parts are the contributions from terms of the type $f_\kappa f_m/f^2$, i.e.,

$$G_s^l(km)=(3/4\pi)\int_0^{2\pi}d\varphi\int_0^{\pi}d\theta\,(F_s^2f_kf_m/f^2)\sin\theta, \quad (4.5)$$

or, more explicitly,

$$G_1^l(km)=(1/35)[12(c_{kk}^l+c_{mm}^l)+4c_{nn}^l]c_{km}^l, \quad (4.6)'$$

$$G_2^l(km)=(1/35)[(c_{kk}^l+c_{mm}^l-2c_{nn}^l)c_{km}^l+2c_{kn}^lc_{nm}^l], \quad (4.6)''$$

where k, m, and n are cyclic over x, y. and z. Thus, we have

$$\{G_s^l(\mathbf{H})\}=\sin^2\Theta\cos^2\Phi\{G_s^l(x)\}+\sin^2\Theta\sin^2\Phi\{G_s^l(y)\}+\cos^2\Theta\{G_s^l(z)\}+2\sin^2\Theta\sin\Phi\cos\Phi G_s^l(xy)+2\sin\Theta\cos\Theta\sin\Phi G_s^l(yz)+2\sin\Theta\cos\Theta\cos\Phi G_s^l(zx), \quad (4.7)$$

$$[G_s^l(\mathbf{H})]=\tfrac{1}{2}(\cos^2\Theta\cos^2\Phi+\sin^2\Phi)\{G_s^l(x)\}+\tfrac{1}{2}(\cos^2\Theta\sin^2\Phi+\cos^2\Phi)\{G_s^l(y)\}+\tfrac{1}{2}\sin^2\Theta\{G_s^l(z)\}+(\cos^2\Theta\sin\Phi\cos\Phi-\sin\Phi\cos\Phi)G_s^l(xy)-\sin\Theta\cos\Theta\sin\Phi G_s^l(yz)-\sin\Theta\cos\Theta\cos\Phi G_s^l(zx). \quad (4.8)$$

In the special cases of $\mathbf{H}\|x$, y, z, of course, these reduce to the results in the previous section, for the limiting case of $\omega_l(\mathbf{H})\tau^l(\mathbf{H})\gg1$.

V. EXPERIMENTAL RESULTS

The measurements were made at the boiling point of liquid hydrogen, $T=20.4$°K. Three samples with different crystallographic orientations, i.e., lengths along the x, y, and z axis, respectively, were cut out from a single crystal ingot by a string saw using nitric acid. The final dimensions of our samples were about 1.5 $\times0.23\times0.2$ cm^3. X-ray analysis showed that the error in orientation was less than 1°. We used one third of the center part of the crystal for welding the probes. For this size of the crystal, end effects are quite small.

Our measurements were carried out using a type K-2 potentiometer and galvanometer. Magnetic fields up to about 7.5 kOe were provided by a water cooled electromagnet with a pole gap of 2.3 in. The current through the samples was usually 0.25 A. We used a potentiometer circuit for adjusting the Hall probes to an equipotential line. Unfortunately this adjustment was somewhat insensitive and may have given rise to appreciable errors in some of the nondiagonal symmetrical components. For the antisymmetric part, however, this insensitivity is relatively unimportant, because the

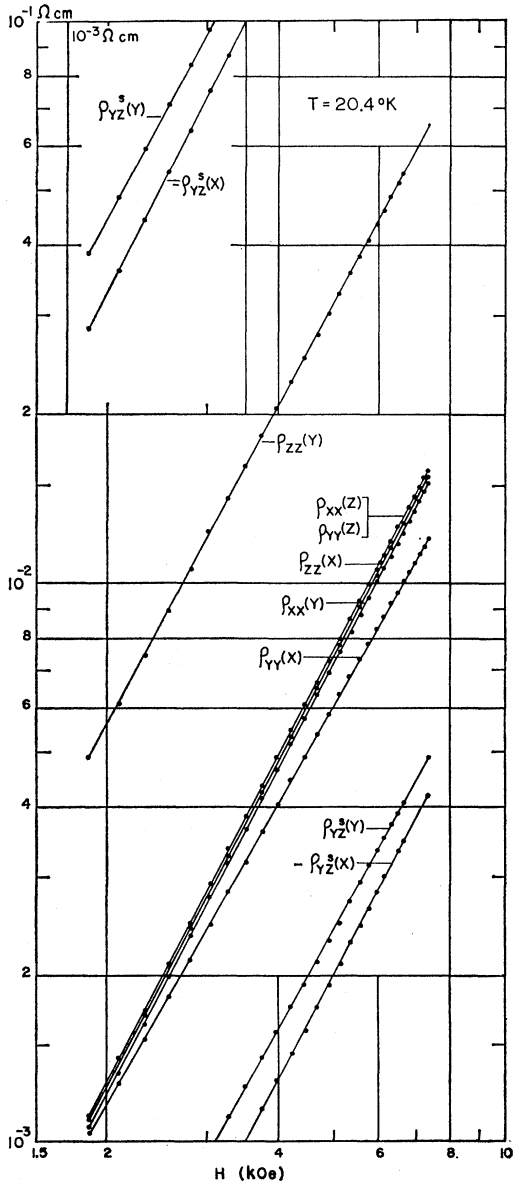

FIG. 2. Experimental curves for the transverse symmetrical tensor components vs H.

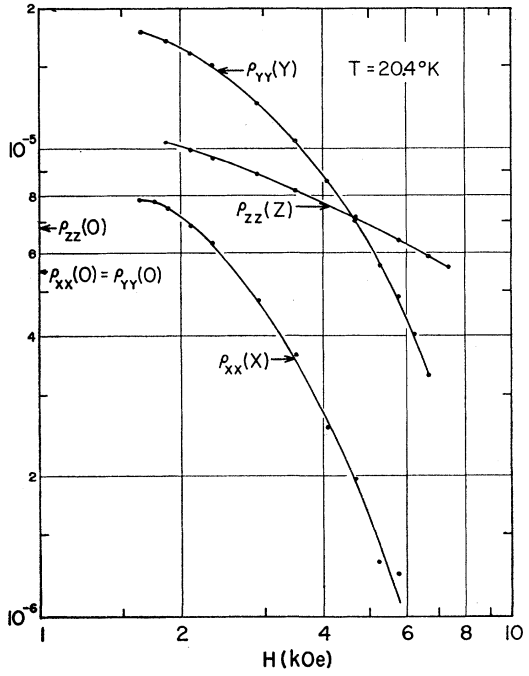

FIG. 3. Experimental curves for the longitudinal tensor components vs H.

magnetoresistance contribution from slight misbalance of the helipot was eliminated by reversing the magnetic field.

Figure 2 shows the experimental symmetric tensor components as a function of H. All the $\rho_{ii}(k)$ $(i \neq k)$ are approximately proportional to $H^{1.86}$. The deviation from proportionality to $H^{2.0}$ was found also in the measurements at liquid helium temperatures.[10] The particularly large value of $\rho_{zz}(y)$ compared to the relatively small values of the other components $\rho_{ii}(k)$ $(i \neq k)$ can be qualitatively understood in terms of the present theory. The unexpectedly large values of $\rho_{yz}{}^{s}(y)$ may not be real but spurious owing to the extremely large magnetoresistance voltage $V_z(y)$ developed by a slight unbalance of the helipot.

Figure 3 shows the variation of the longitudinal tensor with H. The negative magnetoresistance is probably also a spurious effect owing to large probe contact areas. However, the initial values in weak fields may be nearly correct and provide a measure of the saturation values of $\rho_{ii}(i)$. In the absence of a magnetic field, the resistances $\rho_{ii}(0)$ are much smaller than the corresponding $\rho_{ii}(i)$ shown in the same figure. A particularly large value for $\rho_{yy}(y)$ was also found in the measurement at 4°K.[10]

Figure 4 exhibits the antisymmetric tensor components as a function of H. The magnitudes of the $\rho_{ij}{}^{a}(k)$ are considerably different from each other, and the smallest, $\rho_{xy}{}^{a}(z)$, has the steepest slope among all $\rho_{ij}{}^{a}(k)$ at the maximum magnetic field, where the largest, $\rho_{zx}{}^{a}(y)$, has the most gentle slope. In much stronger magnetic fields, we should expect these magnitudes and slopes to approach one another as was found in the measurement at liquid helium temperatures.[10] The sign reversal of $\rho_{xy}{}^{a}(z)$ is to be noted. These characteristic features of the $\rho_{ij}{}^{a}(k)$ are explained in the next section.

Figures 5 to 10 show the angular dependence of $\rho_{ii}(\mathbf{H})$ at fixed $H = 5.76$ kOe. The experimental points, taken every 5°, traced out the curves shown, but were omitted in the final drawing. The figures clearly reveal the symmetry properties of the crystal when the experimental misalignment between H and the crystal axes is taken into account. Figures 5, 8, 9 display reflection symmetry about the x axis, whereas Figs. 6 and 7 are characterized only by inversion symmetry. Figure 10 exhibits 60° symmetry as expected.

It should be pointed out that the experimental values

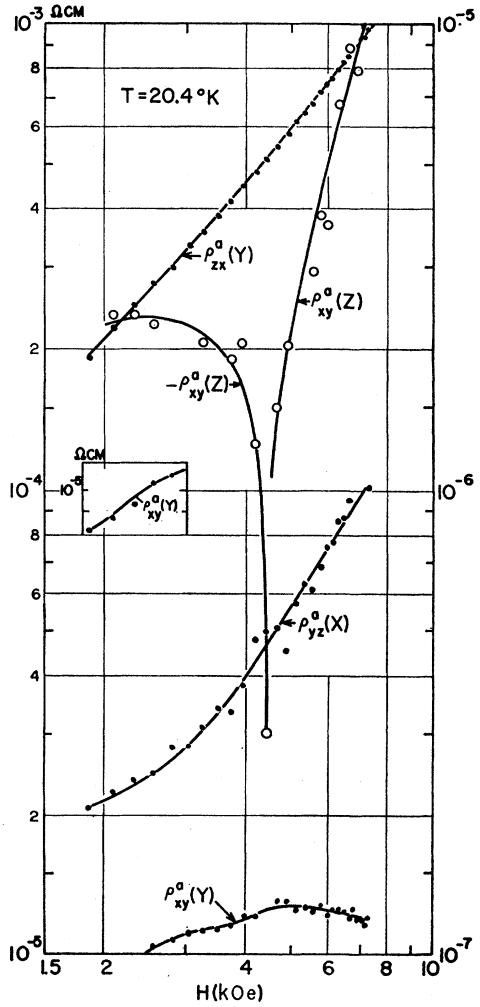

FIG. 4. Experimental curves for the antisymmetric tensor components vs H. The magnitude of $\rho_{xy}{}^{a}(z)$ should be read on the right ordinate.

[10] S. Mase and S. Tanuma, Sci. Repts. Research Inst. Tohoku Univ. A12, 35 (1960).

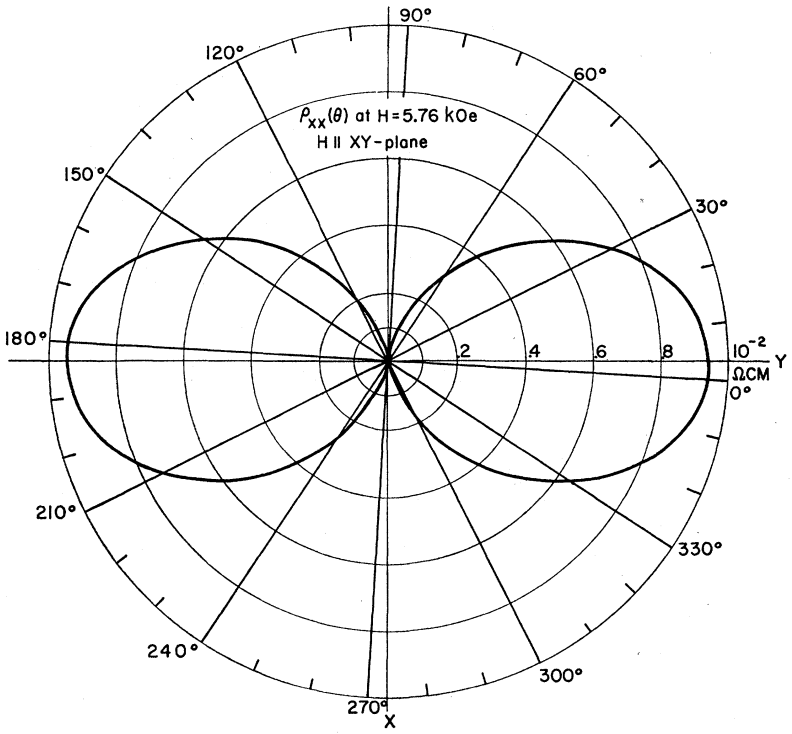

FIG. 5. Angular dependence of $\rho_{zz}(\mathbf{H})$. $\mathbf{H}$ is in xy plane.

of $\rho_{xx}(z)$ using sample Bi I are nearly equal to those of $\rho_{yy}(z)$ using sample Bi II. This result is expected from crystal symmetry and provides additional evidence that our experimental results for large values such as those of $\rho_{ii}(k)$ $(i \neq k)$ are reliable.

VI. COMPARISON BETWEEN EXPERIMENT AND THEORY

In the conductivity expression (4.1) in Sec. V, we did not specify the model but only required ellipsoidal energy surfaces. Now we impose the symmetry

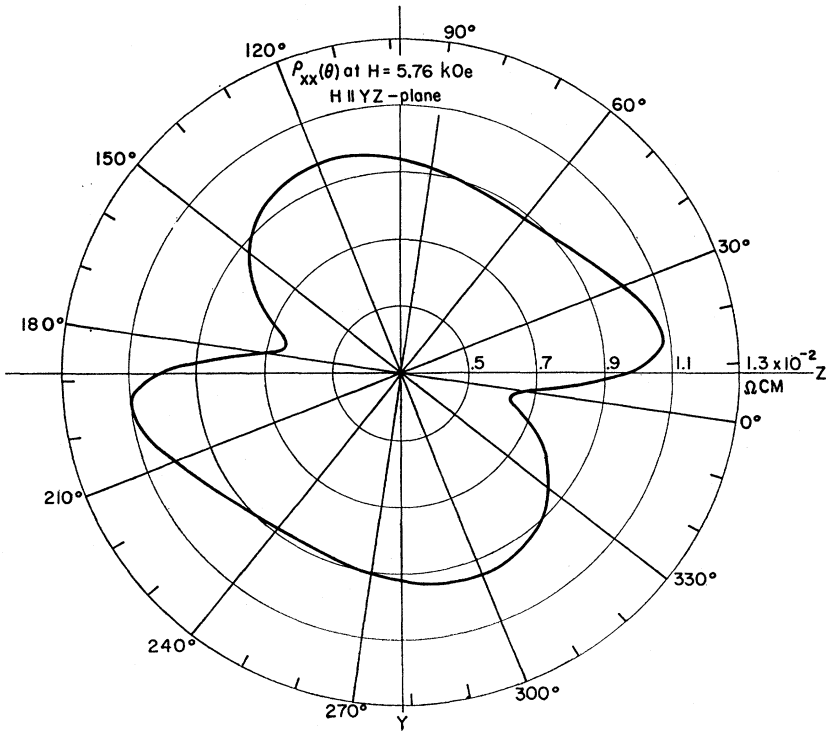

FIG. 6. Angular dependence of $\rho_{zz}(\mathbf{H})$. $\mathbf{H}$ is in yz plane.

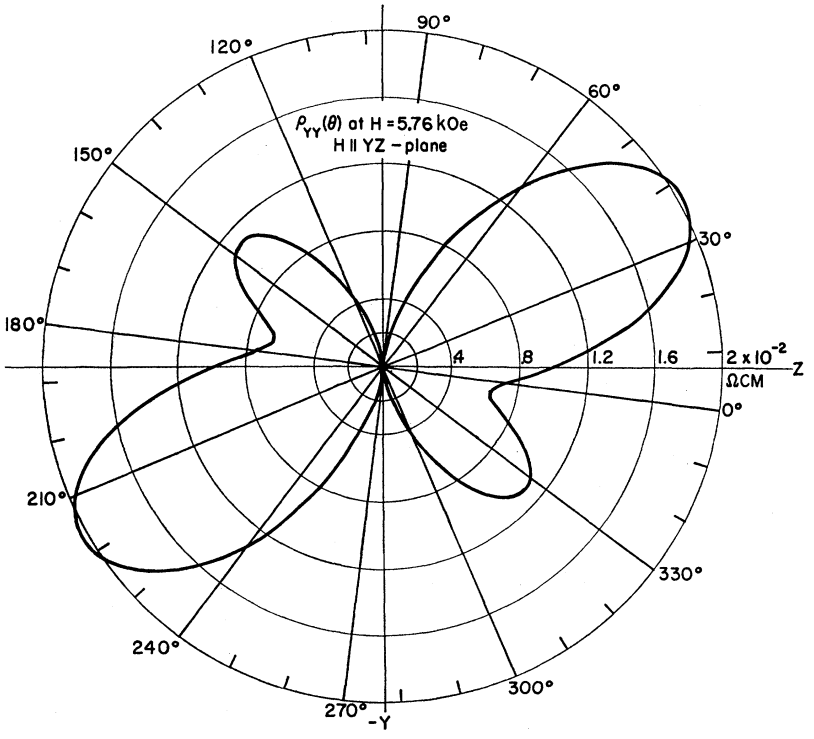

FIG. 7. Angular dependence of $\rho_{yy}(\mathbf{H})$. $\mathbf{H}$ is in yz plane.

requirement on $\alpha_{ij}{}^{l}$ and $c_{ij}{}^{l}$. We adopt the model of 3 (or 6) ellipsoids tilted from the z axis for electrons and 1, (or 2) ellipsoid for holes, as usual. [In the combination of 3 (or 6) ellipsoids for electrons and 2 (or 1) ellipsoids for holes, the result is slightly different.] The pertinent values of $\alpha_{ij}{}^{l}$ and $c_{ij}{}^{l}$ are exhibited in Table I.

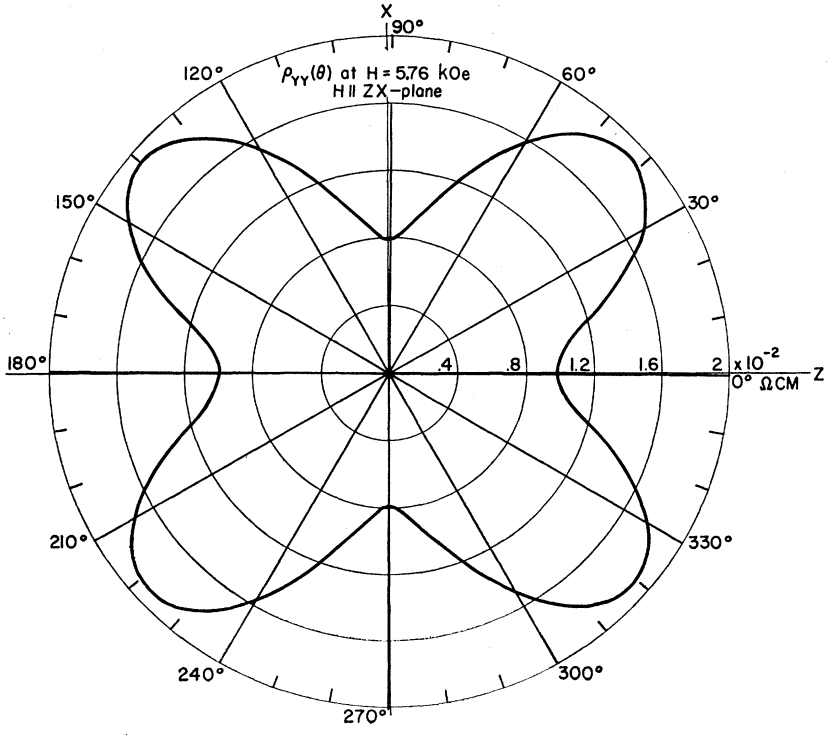

FIG. 8. Angular dependence of $\rho_{yy}(\mathbf{H})$. $\mathbf{H}$ is in zx plane.

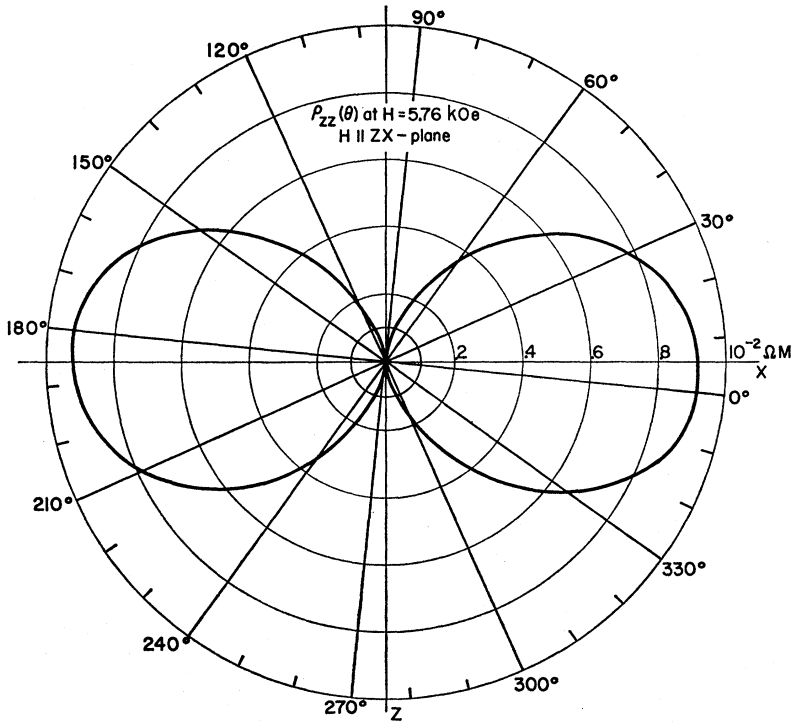

FIG. 9. Angular dependence of $\rho_{zz}(\mathbf{H})$. $\mathbf{H}$ is in zx plane.

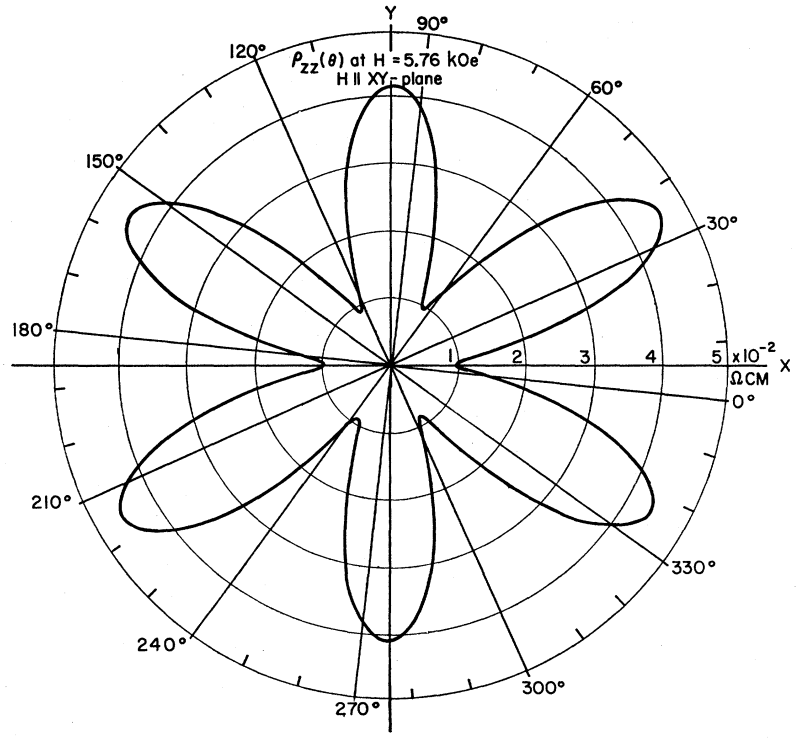

FIG. 10. Angular dependence of $\rho_{zz}(\mathbf{H})$. $\mathbf{H}$ is in xy plane.

Several authors[11] have published experimental values for the Fermi surface parameters α. In the interests of systematic comparison, we use the values from the cyclotron absorption measurements by Galt *et al.*[12]

[11] D. Shoenberg, in *Progress in Low-Temperature Physics*, edited by J. C. Gorter (North-Holland Publishing Company, Amsterdam, 1957), Vol. II; J. E. Aubrey and R. G. Chambers, J. Phys. Chem. Solids **3**, 128 (1957); D. H. Reneker, Phys. Rev. **115**, 303 (1959); G. E. Smith, *ibid.* **115**, 1561 (1959); N. B. Brandt, Soviet Phys.—JETP **10**, 405 (1960); **11**, 975 (1960); W. S. Boyle and A. D. Brailsford, Phys. Rev. **120**, 1943 (1960).

[12] J. K. Galt, W. A. Yager, F. R. Merritt, B. B. Cetlin, and A. D. Brailsford, Phys. Rev. **114**, 1396 (1959).

TABLE I. Parameters $\alpha_{ij}{}^{l}$ and $c_{ij}{}^{l}$ for each energy band.

Band	$\alpha_{11}{}^{l},c_{11}{}^{l}$	$\alpha_{22}{}^{l},c_{22}{}^{l}$	$\alpha_{33}{}^{l},c_{33}{}^{l}$	$\alpha_{12}{}^{l},c_{12}{}^{l}$	$\alpha_{23}{}^{l},c_{23}{}^{l}$	$\alpha_{31}{}^{l},c_{31}{}^{l}$
1	α_1	α_2	α_3	0	α_4	0
2	$\frac{1}{4}(\alpha_1+3\alpha_2)$	$\frac{1}{4}(3\alpha_1+\alpha_2)$	α_3	$\frac{1}{4}\sqrt{3}(\alpha_1-\alpha_2)$	$-\frac{1}{2}\alpha_4$	$\frac{1}{2}\sqrt{3}\alpha_4$
3	$\frac{1}{4}(\alpha_1+3\alpha_2)$	$\frac{1}{4}(3\alpha_1+\alpha_2)$	α_3	$-\frac{1}{4}\sqrt{3}(\alpha_1-\alpha_2)$	$-\frac{1}{2}\alpha_4$	$-\frac{1}{2}\sqrt{3}\alpha_4$
4	β_1	β_1	β_3	0	0	0

The Fermi energy of electrons was taken from Shoenberg's[11] data for the de Haas-van Alphen effect. These are given in Table II. The number of electrons is calculated to be $3.75\times10^{17}/\text{cm}^3$ using Table II. We also need to know the pertinent sound velocities. According to Eckstein, Lawson, and Reneker,[13] the velocities of the longitudinal and the transverse sound waves are both anisotropic. Our theory did not, however, take into account this feature of sound propagation and we shall assume the constants

$$v_1=2.4\times10^5 \text{ cm/sec},$$
$$v_2=1.2\times10^5 \text{ cm/sec}. \tag{6.1}$$

The experimentally determined quantities are the ρ_{ij}, the components of the magnetoresistivity tensor. However, by inversion it is easy to obtain the σ_{ij}, since $\sigma_{ij}=(\rho^{-1})_{ij}$. In principle, the relaxation times $[\tau^l(x)^{-1}]$, $[\tau^l(y)^{-1}]$, and $[\tau^l(z)^{-1}]$ can be determined from the values of $\sigma_{ij}{}^{s}(k)$ $(j\neq k)$ so obtained by use of Eq. (3.34). However, as noted earlier, the values of $\rho_{yz}{}^{s}(x)$ and $\rho_{yz}{}^{s}(y)$ are probably erroneous. We, therefore, neglect the nondiagonal components ρ_{ij} $(i\neq j)$ and calculate $\sigma_{ii}(k)$ $(i\neq k)$ from the experimental values of $\rho_{ii}(k)$ $(i\neq k)$. These approximate values of $\sigma_{ii}(k)$ $(i\neq k)$ when inserted into Eq. (3.34) give a set of linear algebraic relations between the various $[\tau^l(k)^{-1}]$ for any given H. For $H=7.32$ kOe, they are, from $\sigma_{yy}(x)$, $\sigma_{zz}(x)$, $\sigma_{xx}(y)$, $\sigma_{zz}(y)$, and $\sigma_{xx}(z)$, respectively,

$$\begin{aligned}
0.00824K_1(x)+0.00639K_2(x)+K_4(x)&=0.999,\\
K_1(x)+0.0132K_2(x)+0.115K_4(x)&=1.21,\\
0.00318K_1(y)+0.00653K_2(y)+K_4(y)&=0.798,\\
0.0429K_1(y)+0.338K_2(y)+K_4(y)&=2.51,\\
K_1(z)+0.196K_4(z)&=1.99,
\end{aligned} \tag{6.2}$$

where

$$K_l(k)=[\tau^l(k)^{-1}]/\tau_0{}^{-1},$$

TABLE II. Energy surface parameters from the experiments by Galt *et al.*[a] and Shoenberg.[b]

	$\alpha_1{}^{(\mp)}$	$\alpha_2{}^{(\mp)}$	$\alpha_3{}^{(\mp)}$	$\alpha_4{}^{(\mp)}$	$\zeta^{(\mp)}$
Electron	114	1.46	114	10.1	0.0177 eV
Hole	14.7	14.7	1.09	0	0.0117 eV

[a] See reference 12.
[b] See reference 11.

[13] Y. Eckstein, A. W. Lawson, and D. H. Reneker, J. Appl. Phys. **31**, 1534 (1960).

and

$$\tau_0=7\times10^{-11} \text{ sec}.$$

Assuming that $K_2(x)$ and $K_1(y)$ are not large, we find $K_1(x)\sim1.1$, $1\gtrsim K_4(x)\gtrsim0.8$, $5\gtrsim K_2(y)\gtrsim4.4$ from Eq. (6.2), since $K_4(x)=K_4(y)$. By utilizing the experimentally observed sign reversal in $\rho_{xy}{}^{a}(z)$ and Eq. (4.1) in conjunction with Eq. (6.2), we find $K_1(z)\sim1.81$, $K_4(z)\sim0.93$. Because $K_2(x)$ and $K_1(y)$ do not make significant contributions in Eq. (6.2), their values are indeterminate. As can be seen from the left-hand terms of the first and third equations of (6.2), the theory predicts that $\sigma_{yy}(x)$ should be nearly equal to $\sigma_{xx}(y)$, but experimentally this is not the case. Because of this disagreement, $K_4(x)$ and $K_2(y)$ are indeterminate in the range of the above limits. We now choose values for the deformation potential anisotropy constants c_i and d_i in close accordance with the foregoing restrictions on $K_l(k)$.

The unique conclusion from $K_1(x)<K_1(z)$ is that c_1, $c_3\gg c_2$, c_4 in correspondence with experimental finding that α_1, $\alpha_3\gg\alpha_2$, α_4. If the theoretical value of $\sigma_{xx}(y)$ is taken to be in accordance with the experimental value, i.e., if we assume that $K_4(x)<K_4(z)$, it follows that $d_1>d_3$, corresponds to the experimental result that $\beta_1>\beta_3$. It was not possible, however, to find values of c_i and d_i, giving values of $K_2(y)\gtrsim4.4$. The small experimental value of $\rho_{zz}(y)$ (despite the fact that this component is much larger than any other) appears to be responsible for this discrepancy with the theory. Nevertheless, our best estimates for c_i and d_i are as follows: $c_1=3$, $c_2=0.02$, $c_3=1$, $c_4=0.1$, $d_1=0.9$, and $d_3=0.3$. Using these values and the values of α_i, β_i, n^-, v_s, $n^--n^+/n^-=5.2\times10^{-4}$, and $D=2.72$ eV, we find the following values for the various $\tau^l(k)$:

$$\begin{aligned}
\tau^{(1)}(x)&=5.75\times10^{-11} \text{ sec},\\
\tau^{(2)}(x)&=4.32\times10^{-11} \text{ sec},\\
\tau^{(4)}(x)&=8.78\times10^{-11} \text{ sec},\\
\tau^{(1)}(y)&=3.99\times10^{-11} \text{ sec},\\
\tau^{(2)}(y)&=5.18\times10^{-11} \text{ sec},\\
\tau^{(4)}(y)&=\tau^{(4)}(x),\\
\tau^{(1)}(z)&=3.87\times10^{-11} \text{ sec},\\
\tau^{(4)}(z)&=7.53\times10^{-11} \text{ sec}.
\end{aligned} \tag{6.3}$$

We note that anisotropy in $\tau^l(k)$ is not nearly as pronounced as the anisotropy in α_i, c_i, and d_i. Although the relaxation times for the holes are larger than those

for the electrons, the difference is not as large as suggested by Aubrey and Chambers.[11] Rough measurements of $\rho_{xx}(0)$ as a function of temperature indicate that the relaxation times are approximately a factor of 10 larger at liquid helium temperatures than those reported here for 20.4°K. Such values would be consistent with those estimated by Galt *et al.*[12] from their cyclotron resonance experiments.

Using the values of the various parameters given above, we may now calculate the field dependence of the ρ_{ik}. These theoretical curves are exhibited in Figs. 11–13. As mentioned above, the curves for $\rho_{xx}(y)$ and $\rho_{xx}(z)=\rho_{yy}(z)$ were fitted to the data at $H=7.32$ kOe and the curve for $\rho_{xy}{}^a(z)$ was fitted at its zero. Despite the discrepancies between theory and experiment noted above, the general features of the theoretical curves are very similar to the observed behavior shown in Figs.

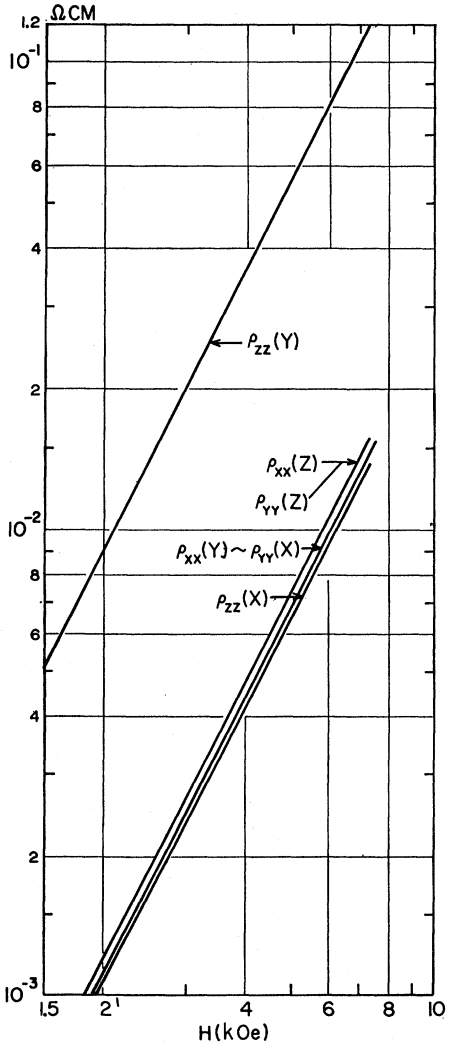

FIG. 11. Theoretical curves for the transverse symmetric components $\rho_{ii}(k)$ vs H.

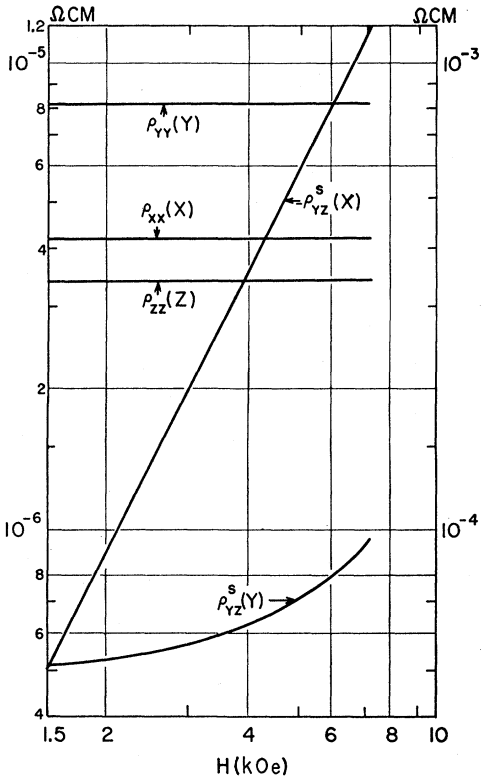

FIG. 12. Theoretical curves for the longitudinal components and $\rho_{yz}{}^s(x)$ and $\rho_{yz}{}^s(y)$. The magnitude of $\rho_{yz}{}^s(x)$ should be read on the right ordinate.

2–4 except for the behavior of $\rho_{yz}{}^s(y)$ which we believe to be spurious. Numerical discrepancies as large as a factor of 3 occur in some cases. In the case of the nondiagonal components, such differences may be ascribed, at least in part, to experimental error. This explanation is not valid however in the case of $\rho_{yy}(x)$, $\rho_{zz}(x)$, and $\rho_{zz}(y)$, nor can it explain why $\rho_{ii}(k)$ $(i\neq k)$ varies as $H^{1.86}$ rather than $H^{2.0}$. In the case of impure crystal, the $\sigma_{ij}{}^a(k)$ $(i\neq j\neq k)$ terms contribute greatly to the deviation from $H^{2.0}$ dependence of $\rho_{ij}(k)$ $(i\neq k)$, but this is not the case here because $\sigma_{ij}{}^a(k)$ is negligibly small. These discordances between theory and experiment suggest that our model is difficient in some respects. It may be necessary to take into account the departure of the energy surfaces from the ellipsoid, the anisotropy of the sound waves, the optical branch of the phonon spectrum, and intervalley and interband transitions. Most of these effects, unfortunately, are difficult to treat. We should emphasize, however, that this simple model does explain the large value of $\rho_{zz}(y)$ compared to the relatively small values of $\rho_{ii}(k)$ $(i\neq k)$, the wide variation and correct order of magnitudes of $\rho_{ij}{}^a(k)$ $(i\neq j\neq k)$, the sign reversal of $\rho_{xy}{}^a(z)$ and the relatively large value of $\rho_{yy}(y)$ compared to $\rho_{xx}(x)$ and $\rho_{zz}(z)$.

It is of interest to point out that the order of magni-

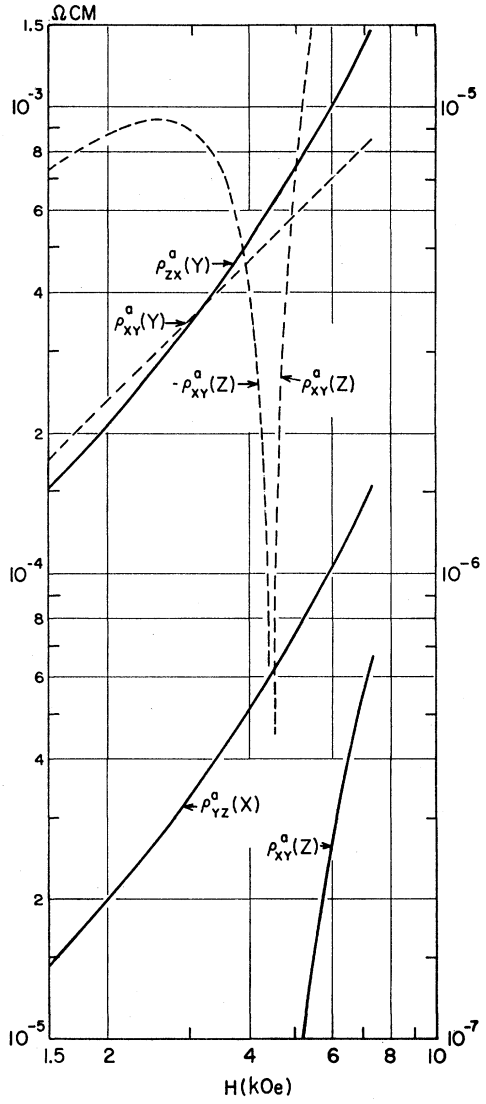

FIG. 13. Theoretical curves for the antisymmetric components vs H. The dashed curves should be read on the right ordinate.

tude of antisymmetric components can be explained only if the ratio of the difference in concentration of electrons and holes to the concentration of electrons is about 5×10^{-4} (since the concentration of electrons is only about 2×10^{-5} per atom in bismuth, the result bespeaks an impurity concentration of the order of 10^{-8} per atom) and if these carriers all have very large $\omega_c\tau$. Several authors[14] have suggested that to explain the large value of the specific heat and the effect of doping on the de Haas-van Alphen effect it is necessary to invoke two hole bands, one light and one heavy. The data presented here appear to be inconsistent with this possibility. The theory presented here is only consistent with the experimental values of the antisymmetric

[14] I. N. Kalinkina and P. G. Strekov, reference 4; D. Weiner, Phys. Rev., **125**, 1226 (1962).

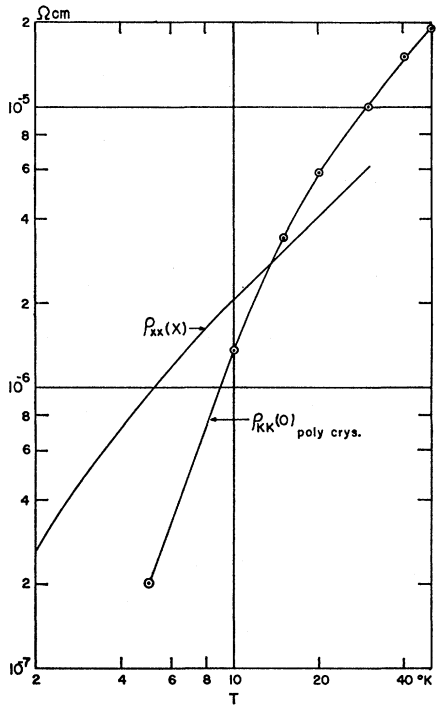

FIG. 14. Theoretical temperature dependence of $\rho_{xx}(x)$ and experimental result for the resistance of a polycrystal in zero field by White and Wood (reference 15).

components, provided that there are no heavy holes. If heavy holes are present, and if the condition $\omega_c\tau\gg1$ is satisfied for both electrons and holes at the temperature and magnetic fields considered, these components should be far larger than those observed and the dependence on magnetic field would be quite different.

Although we have not derived an expression for the conductivity tensor for zero magnetic field, we anticipate that its components will have nearly the same temperature dependence as those for $\rho_{ii}(i)$ in a strong magnetic field. In Fig. 14, we show the theoretical temperature dependence for $\rho_{xx}(x)$ at $H=7.3$ kOe as well as the experimental results of White and Woods[15] for polycrystals. The theory predicts a linear dependence of $\rho_{xx}(x)$ down to 10°K, while the experimental curve shows a sharp break at about 20°K. The very different behavior of the experimental curve from the Gruneisen formula (3.37) suggests again that other types of scattering than those considered here are playing an appreciable role.

Finally, we should remark that the sign reversal for $\rho_{xy}{}^a(z)$ is determined by the condition

$$\omega(z)^2\tau(z)^2[(n^--n^+)/n^-)]=\text{const}, \qquad (6.4)$$

or the critical field H_c is

$$H_c\propto[(n^--n^+)/n^-]^{-\frac{1}{2}}\tau(z)^{-1}$$
$$\propto TJ(x)[(n^--n^+)/n^-]^{-\frac{1}{2}}. \qquad (6.5)$$

[15] G. K. White and S. B. Woods, Phil. Mag. **3**, 342 (1958).

However, because $J(x)$ experimentally has a sharper dependence on T than predicted, we must expect H_c to decrease more rapidly with T than predicted by Eq. (6.5). In the residual resistance range, however, H_c should become temperature independent. To date, the sign reversal at liquid helium temperatures has not been found. In our sample, the expected H_c is much smaller than 0.44 kOe, the smallest field available to us. At liquid nitrogen temperatures, H_c should be about 17 kOe, also inaccessible to us. Some tendency toward a reversal is descernible in the data of Connel and Marcus.[1]

ACKNOWLEDGMENTS

One of the authors (S.M.) wishes to express his sincere thanks to Professor M. H. Cohen for his warm hospitality and valuable advice at the University of Chicago.

PHYSICAL REVIEW VOLUME 127, NUMBER 4 AUGUST 15, 1962

Electrical Properties of *n*-Type Gallium Arsenide

D. J. OLIVER
Services Electronics Research Laboratory, Baldock, England
(Received January 3, 1962)

As part of a general investigation into the properties of gallium arsenide, the Hall coefficient and resistivity of three pure samples have been measured from 300 to 2°K. The highest mobility measured at 300°K was 7200 cm²/V-sec increasing to 22 000 cm²/V-sec at 72°K, the mobility temperature curve following the theory of Ehrenreich very closely. At helium temperatures impurity conduction was observed with the resistivity $\rho \propto \exp(-\epsilon_1/kT)$ and ϵ_1 varying from 9.8×10^{-5} eV to 5.8×10^{-4} eV. A discussion of these results is given in terms of the theory of Miller and Abrahams and Twose.

In one sample, below about 30°K the current was not a linear function of the voltage. This arises from a dependence of mobility on applied electric field and because carriers can be excited from impurity states to the conduction band. An analysis of the energy loss processes for electrons suggest that piezoelectric scattering is the most important mechanism below about 30°K but that above this temperature optical scattering is dominant. Impact ionization occurs between 4 and 12°K.

A. INTRODUCTION

MEASUREMENTS of the electrical properties of a semiconductor provide much basic information on their properties and particularly on the mechanisms of charge transport and the nature of the scattering processes. This paper describes some measurements of Hall coefficient and conductivity, on samples of low resistivity *n*-type gallium arsenide over the temperature range 300 to 2°K. Previous investigations have been adequately described in the book by Hilsum and Rose-Innes,[1] but the results described here have been obtained on purer material than was previously available and are thus of special interest.

The discussion of the experimental results falls naturally into three sections. The material available was pure enough for the mobility above about 60°K to be determined largely by lattice scattering. Ehrenreich[2] has recently calculated the theoretical temperature dependence of electron mobility in gallium arsenide on the assumption that scattering by the polar optical modes is the dominant lattice process and our results therefore provide a convenient check on this theory, the agreement being very satisfactory.

At low temperatures the measurements show evidence of impurity conduction in a more pronounced way than has previously been possible in *n*-type gallium arsenide. The results illustrate the difference between the two possible types of impurity conduction, the "hopping" process which occurs for low impurity concentrations and the metallic type of conduction which takes place in less pure samples.

In one sample at low temperatures, departures from Ohm's law were observed, and to explain these results a discussion is given of the various mechanisms by which electrons lose energy and also of the possibility of electrons being transferred from impurity states to the conduction band under the action of an electric field.

B. EXPERIMENTAL TECHNIQUE

The specimens used were rectangular bars (typically 0.6-×0.2-×0.1-cm), cut from single crystal material. After grinding, etching ($1H_2O\ 3H_2SO_4/1H_2O_2$), and washing in de-ionized water, six contacts were formed on the specimen by alloying to it small pellets of indium. Reliable low-resistance Ohmic contacts could readily be made in this way.

A large number of specimens have been examined from room temperature to liquid nitrogen temperature using the simple apparatus described by Ure.[3]

[1] C. Hilsum and A. C. Rose-Innes, *Semiconducting* III–V *Compounds* (Pergamon Press, New York, 1961).
[2] H. Ehrenreich, Phys. Rev. **120**, 1951 (1960).
[3] R. W. Ure, Rev. Sci. Instr., **28**, 836 (1957).